Bulletin of Mathematical Biology manuscript No.
(will be inserted by the editor)

arXiv:0804.2352v1 [q-bio.QM] 15 Apr 2008

J. T. Locsei · T. J. Pedley

Run and tumble chemotaxis in a shear flow: the effect of temporal comparisons and other complications

Received: date / Accepted: date

Abstract *Escherichia coli* is a motile bacterium that moves up a chemoattractant gradient by performing a biased random walk composed of alternating runs and tumbles. This paper presents calculations of the chemotactic drift velocity v_d (the mean velocity up the chemoattractant gradient) of an *E. coli* cell performing chemotaxis in a uniform, steady shear flow, with a weak chemoattractant gradient at right angles to the flow. Extending earlier models, a combined analytic and numerical approach is used to assess the effect of several complications, namely (i) a cell cannot detect a chemoattractant gradient directly but rather makes temporal comparisons of chemoattractant concentration, (ii) the tumbles exhibit persistence of direction, meaning that the swimming directions before and after a tumble are correlated, (iii) the cell suffers random re-orientations due to rotational Brownian motion, and (iv) the non-spherical shape of the cell affects the way that it is rotated by the shear flow. These complications influence the dependence of v_d on the shear rate γ. When they are all included, it is found that (a) shear disrupts chemotaxis and shear rates beyond $\gamma \approx 2\mathrm{s}^{-1}$ cause the cell to swim down the chemoattractant gradient rather than up it, (b) in terms of maximising drift velocity, persistence of direction is advantageous in a quiescent fluid but disadvantageous in a shear flow, and (c) a more elongated body shape is advantageous in performing chemotaxis in a strong shear flow.

Keywords Chemotaxis · Shear flow · Random walk · Escherichia coli

Mathematics Subject Classification (2000) 62P10 · 82B41 · 92B05 · 76Z10

J. T. Locsei is supported by an Oliver Gatty Studentship from the University of Cambridge.

J. T. Locsei
Department of Applied Mathematics and Theoretical Physics, University of Cambridge, Cambridge CB3 9EW, U.K.
E-mail: j.t.locsei@damtp.cam.ac.uk

T. J. Pedley
Department of Applied Mathematics and Theoretical Physics, University of Cambridge, Cambridge CB3 9EW, U.K.

1 Introduction

Free swimming bacteria are present in many naturally occurring aqueous environments including animal intestines (enteric bacteria) and the open ocean (marine bacteria). In the ocean, motility could influence bacterial ecology and the role of bacteria in oceanic biogeochemistry [19]. Thus there is an oceanographic motivation to understand how motile bacteria behave in a weakly turbulent, sheared environment. Bacteria are also known to adhere to each other and/or other surfaces and form biofilms [13]. To understand the formation of biofilms in the presence of a fluid flow it may be helpful to model the motion of free swimming bacteria in the sheared region adjacent to the biofilm.

In this paper we focus on modelling *Escherichia coli*, which is the most well studied motile bacterium. As described by Berg [6], *E. coli* is a common enteric bacterium with a rod shaped body $\approx 1\ \mu$m in diameter and $\approx 2\ \mu$m long. A typical *E. coli* cell has ≈ 6 left-handed helical flagella emerging from random points on the sides of its body, each of them extending several body-lengths into the surrounding fluid. The flagella are powered by reversible rotary motors. When all the flagella spin counter-clockwise, they form a synchronous bundle and propel the cell forward in an almost-straight ‘run’. When one or more flagella spin clockwise, the flagellar bundle comes apart and the cell swims in a highly erratic ‘tumble’, with little net displacement but a large change in direction. Tumbles exhibit ‘persistence of direction’, meaning that the swimming directions before and after a tumble are correlated, with a mean angle between the new and previous swimming directions of $\approx 62^{\mathrm{o}}$ [8]. Hereafter, for brevity, ‘persistence of direction’ shall be referred to simply as ‘persistence’.

Even during a run, the cell exhibits small, random changes in direction, and these have been attributed to rotational Brownian motion (*i.e.* thermal collisions with molecules in the surrounding fluid). Berg [6] estimated the coefficient of Brownian rotation to be $D_{\mathrm{R}} \approx 0.062$ radians^{2}s^{-1} for an *E. coli* cell swimming in a fluid of viscosity 2.7 cp at 32$^{\mathrm{o}}$C, and this is consistent with experimental observations [8]. However, this estimate was based on treating the *E. coli* cell as a sphere of diameter 2 μm, and when one takes into account the stabilising effect of the flagellar bundle, the theoretically predicted coefficient of Brownian rotation is an order of magnitude smaller than the observed rotational diffusivity [17], so it seems likely that the observed diffusivity is in fact due to intrinsic ‘wobbly swimming’ rather than true (thermal) Brownian rotation [7].

An *E. coli* cell performs chemotaxis (*i.e.* swims up a chemoattractant gradient) by alternately running and tumbling and biasing the length of the runs. The run durations are exponentially distributed with a rate constant (‘tumble rate’) of $\lambda \approx 1$ s^{-1}, and a corresponding mean run duration of $\lambda^{-1} \approx 1$ s [8]. Tumble durations are also exponentially distributed but with a much shorter mean duration of ≈ 0.1 s. An *E. coli* cell is too small to detect spatial differences in the concentration of a chemoattractant on the scale of the cell length, so it performs temporal comparisons instead. It continually ‘measures’ the concentration of chemoattractants (typically nutrients) in its environment such as serine and aspartate. If the concentration over the past second is higher than the concentration over the previous three seconds, the tumble rate is reduced and the expected run length is extended. Thus, the cell performs a biased random walk and gradually drifts toward regions of high chemoattractant concentration. The cell's mean velocity up the chemoattractant gradient is termed the 'drift velocity'.

There have been a number of theoretical studies on run and tumble chemotaxis with no background flow [29, 14, 15, 16, 12, 25], and on the role of bacterial shape in chemotaxis [33, and references therein]. Some theoretical work has also been published on run and tumble chemotaxis with background flows. Bowen et al [10] simulated bacterial chemotaxis toward a neutrally buoyant phytoplankton cell exuding dissolved organic carbon in an unsteady shear flow. Luchsinger et al [26] simulated a similar situation, but also investigated the case in which bacteria reverse direction rather than tumble. Bearon and Pedley [5] and Bearon [4] developed an advection-diffusion equation describing run and tumble chemotaxis in a shear flow. The work of Bearon and Pedley [5] provided a particular motivation for the present study, since it showed that time-delays in the bacterial response can have a strong effect on drift velocity in a shear flow.

The present work is in one sense an extension of Locsei [25] to include shear flows, and in another sense an extension of Bearon and Pedley [5] to include temporal comparisons, non-spherical cell shape, persistence, and Brownian rotation. Section 2 introduces the model and its basic assumptions, and section 3 describes in more detail the response function that is used to model the temporal comparisons performed by the cell. Section 4 presents a general analytic framework for calculating the drift velocity. The remainder of the paper is devoted to specific calculations of the drift velocity while taking account of (i) temporal comparisons performed by the cell, (ii) persistence of direction, (iii) Brownian rotation, and (iv) non-spherical cell shape. The drift velocity under the combined effects (i), (ii) and (iii) is computed analytically in section 5, and the drift velocity under the combined effects (i) and (iv) is computed semi-analytically in section 6. The case where all effects (i)–(iv) are present is treated numerically by Monte Carlo simulation in section 7. Section 8 summarises the key findings.

2 Outline of model

Consider a cell performing run and tumble chemotaxis, swimming in an unbounded fluid with a chemoattractant concentration gradient $\nabla c \parallel \hat{\boldsymbol{z}}$ and with a background shear flow $\boldsymbol{u} = \gamma z \hat{\boldsymbol{x}}$ where $\hat{\boldsymbol{x}}$ and $\hat{\boldsymbol{z}}$ are unit vectors in the x and z directions and γ is the shear rate. For convenience, we shall frequently parameterise the strength of the shear flow by $\Omega = \gamma/2$ rather than γ. We assume that during a run the cell swims at constant speed v_s relative to the fluid. The cell's swimming direction is described by a unit vector $\boldsymbol{e}$ that changes with time due to tumbles, Brownian rotation, and the shear flow.

During a run, the probability that the cell tumbles in the next time interval dt is $\lambda(t)dt$, where λ is the 'tumble rate'. We assume that the cell alters its tumble rate linearly in response the chemoattractant, according to

$$\lambda(t) = \lambda_0 \left[1 - \Delta(t)\right], \tag{1}$$

where $\lambda_0 = 1\mathrm{s}^{-1}$ is the baseline tumble rate, and the fractional change in tumble rate is given by

$$\Delta(t) = \int_{-\infty}^{t} c(t')R(t-t')dt', \tag{2}$$

where $c(t')$ is the chemoattractant concentration experienced by the cell at time t', and R is the cell's 'response function'. R may be thought of as the impulse response of the tumble rate, since it describes the way that λ changes when the cell is subject to a delta function impulse of chemoattractant concentration. The form of tumble modulation given by (2) has been used in several earlier models [29, 14, 12, 25] and it is motivated by the experimental results of [9] and [30]. The form of R is discussed in section 3. Our analysis will be restricted to 'weak chemotaxis', meaning small fractional changes in the tumble rate, *i.e.* $|\Delta(t)| \ll 1$. Physically, weak chemotaxis corresponds to a shallow chemoattractant gradient.

Brownian rotation causes random re-orientation of the cell swimming direction, so that in between tumbles the probability density function f of the swimming direction $\boldsymbol{e}$ evolves according to the Fokker-Planck equation

$$\frac{\partial f}{\partial t} + \nabla_{\boldsymbol{e}} \cdot [\boldsymbol{\omega}(\boldsymbol{e}) \times \boldsymbol{e} f] = D_{\mathrm{R}} \nabla_{\boldsymbol{e}}^2 f, \tag{3}$$

where $\boldsymbol{\omega}(\boldsymbol{e})$ is the deterministic angular velocity of the cell due to the shear flow, D_{R} is the rotational diffusion coefficient and $\nabla_{\boldsymbol{e}}$ is the gradient operator in direction space. The form of $\boldsymbol{\omega}(\boldsymbol{e})$ depends on what assumptions are made about the cell shape. As discussed in the introduction, the rotational diffusivity of the cell may be due to intrinsic randomness in its swimming motion, rather than true Brownian rotation. Throughout this paper we shall set either $D_{\mathrm{R}} = 0$ or $D_{\mathrm{R}} = 0.062$ radians^{2}s^{-1}, where the latter value is consistent with what has been measured in experiments on *E. coli* [6].

When a cell tumbles, its choice of new direction is governed by a probability distribution which is axisymmetric about the initial direction. We allow for the tumbles to exhibit directional persistence, so that the expected scalar product of the swimming directions $\boldsymbol{e}(0^-)$ and $\boldsymbol{e}(0^+)$ immediately before and after a tumble at time $t = 0$ is given by

$$E[\boldsymbol{e}(0^-) \cdot \boldsymbol{e}(0^+)] = \alpha_{\mathrm{p}}, \tag{4}$$

where E denotes an expectation value and α_{p} is the 'persistence parameter'. Experimentally, $\alpha_{\mathrm{p}} \approx 0.33$ [6]. We treat tumbles as instantaneous and neglect any rotation of the cell caused by the shear flow during the tumble.

Our aim is to calculate the chemotactic drift velocity. Let z_{f} be the z location of a cell at the end of a run, relative to its position at the beginning of the run, and let t_{f} be the duration of a run. Since we treat tumbles as instantaneous, the chemotactic drift velocity v_{d} is

$$v_{\mathrm{d}} = E[z_{\mathrm{f}}]/E[t_{\mathrm{f}}]. \tag{5}$$

While our model assumes an unbounded domain, we note that for a cell swimming in a bounded domain of length $\gg v_{\mathrm{s}}/\lambda_0$, v_{d} provides a measure of the transient velocity up the chemoattractant gradient before the cell encounters the boundaries.

3 Response function

In writing (2), we assume that the tumble rate is a linear functional of the concentration history seen by the cell. The validity of this assumption has never been

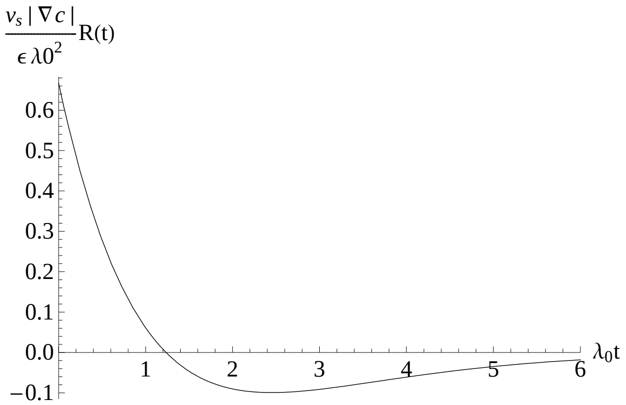

Fig. 1 The response function used in the results section of this paper, originally proposed by Clark and Grant [12].

directly assessed, and the chemotactic response function R has never been directly measured. However, experiments by Block et al [9] and Segall et al [31] indicate that the bias of a single flagellar motor (the probability of counter-clockwise rotation) is a linear functional of the concentration history, thus providing indirect evidence for (1). These authors monitored the direction of rotation of a single rotary motor on an *E. coli* cell while delivering small impulses of chemoattractant to the fluid around the cell. Repeating the experiment multiple times and with different cells, the experimenters determined the motor bias as a function of time (see for example figure 1 of Segall et al [31]). The impulse response of the motor bias is double-lobed, with the bias rising above the baseline for the first ≈ 1 s after the delivery of the impulse, falling below the baseline for the following ≈ 3 s, and then returning to baseline. The two lobes of the response have equal area. Furthermore, it was found that the responses to other time-series of stimuli (*e.g.* ramp or sinusoidal changes in chemoattractant concentration) are consistent with the cell behaving as a linear system, so that the motor bias is well described by the convolution integral of the stimulus with the impulse response (*c.f.* equation 1). The primary exception to this linear behaviour is that for small changes in chemoattractant concentrations, cells respond to increases in concentration but not to decreases; we neglect this nonlinearity in our analysis.

Following the lead of previous papers [29, 14, 12], we adopt the view that in the absence of experimental measurements of R, a convenient assumption is that R has a similar shape to the impulse response of the individual motor bias reported in Block et al [9] and Segall et al [31]. This means that (i) R should be composed of a positive lobe followed by a negative lobe of equal area so that

$$\int_0^\infty R(t)\,dt = 0, \tag{6}$$

and (ii) $R(t)$ should decay to zero for t greater than about 4 s. An additional constraint is that R must be small enough for our linear analysis to be valid. Certainly,

R must be small enough that λ never becomes negative, which necessitates

$$\varepsilon \equiv |\Delta(t)|_{\max} = v_{\mathrm{s}} |\nabla c| \left| \int_0^\infty t\, R(t)\, dt \right| < 1. \tag{7}$$

The analysis that will be presented in this paper is asymptotically accurate as $\varepsilon \to 0$.

We shall use the response function

$$R(t) = \frac{2\varepsilon\lambda_0^2}{3v_{\mathrm{s}}|\nabla c|}\, \mathrm{e}^{-\lambda_0 \mathrm{t}} [1 - \lambda_0 \mathrm{t}/2 - (\lambda_0 \mathrm{t}/2)^2], \tag{8}$$

with $\varepsilon \ll 1$ in order for our linear analysis to be valid. This R, plotted in figure 1, is a theoretically motivated response function proposed by Clark and Grant [12] that has the above-mentioned properties (i) and (ii), and it matches the experimentally measured motor bias reasonably well. It may seem odd that $|\nabla c|$ appears on the right hand side of (8), since R is a property of the cell rather than its environment. However the factor of $1/|\nabla c|$ in R simply reflects the fact that we have used ε to parameterise the strength of the combined effect of the cell's response R and the chemoattractant gradient ∇c on $\Delta(t)$. Note that in the computations we do not have to specify a value for $|\nabla c|$, since R and $|\nabla c|$ appear together as a product in the equation for $\Delta(t)$.

4 Partial calculation of drift velocity v_{d}

In this section we present the first part of the analytic drift velocity calculation, which is common to both the spherical and non-spherical cell cases. Calculating v_{d} is non-trivial because of the interdependence of the tumble rate and the path taken by the cell. The tumble rate at any time depends in principle on the entire path history of the cell through (2), while the path of the cell depends in turn on the tumble rate. The method of solution is the same as that used in Locsei [25], so we shall omit some details. As noted earlier, in order to make the analysis tractable, our analysis will be restricted to weak chemotaxis, *i.e.* $0 \leq |\Delta(t)| \ll 1$. In this case, the expectation values of the run displacement z_{f} and duration t_{f} satisfy $E[z_{\mathrm{f}}] = v_{\mathrm{s}}\lambda_0 O(\Delta)$ and $E[t_{\mathrm{f}}] = [1 + O(\Delta)]/\lambda_0$, so, from (5),

$$v_{\mathrm{d}} = \lambda_0 E[z_{\mathrm{f}}] + v_{\mathrm{s}} O(\Delta^2). \tag{9}$$

We shall neglect terms that are $O(\Delta^2)$.

Consider a run commencing at time $t = 0$ at location $z = 0$. During the run, the cell swims in a random walk governed by rotational Brownian motion until the run terminates with a tumble at time t_{f}. Note that the expected stopping location of a terminated random walk with a stopping rate λ_{stop} is the same as the expected first event location on an unterminated walk with an event rate $\lambda_{\mathrm{event}} = \lambda_{\mathrm{stop}}$. Thus, in calculating $E[z_{\mathrm{f}}]$, it is permissible to treat tumbles for $t > 0$ as events that have no effect on the cell's motion, and treat the tumble at $t = t_{\mathrm{f}}$, $z = z_{\mathrm{f}}$ as a first event (the first tumble in $t > 0$). The utility of this treatment is that we may conceptually break the expectation E in $E[z_{\mathrm{f}}]$ into two consecutive operations. First, assuming a given path $z(t) : -\infty < t < \infty$ taken by the cell, one calculates the conditional expectation of z_f for that path. Second, one takes the expectation over all such paths to obtain $E[z_\mathrm{f}]$, with the understanding that in the $t \leq 0$ section of a path the cell is subject to reorientations due to both Brownian motion and tumbles, whereas in the $t > 0$ section of a path the cell is subject to reorientation due to Brownian motion alone. Writing out the two expectations in symbolic notation,

$$E[z_\mathrm{f}] = E_\mathrm{paths}\left[\int_0^\infty dt\, z_\mathrm{path}(t) p_\mathrm{path}(t)\right], \tag{10}$$

where the E_paths denotes an expectation over paths, $z_\mathrm{path}(t)$ denotes the position of the cell at time t on a particular path, and $p_\mathrm{path}(t)$ is the probability density function for the tumble time t_f on a particular path. Since tumbles for $t > 0$ are treated as having no effect on cell motion, paths are independent of t_f and one is free to take the path expectation inside the integral over tumble times. Substituting (10) into (9) and dropping the 'path' subscript for brevity, one then has

$$v_\mathrm{d} = \lambda_0 \int_0^\infty dt\, E[z(t)p(t)]. \tag{11}$$

The probability density function p(t) for the tumble time is given by

$$p(t) = \lambda(t) \exp\left[-\int_0^t \lambda(t')\, dt'\right], \tag{12}$$

where $\lambda(t)$ is the path-dependent tumble rate at time t, given by (1).

We shall calculate the drift velocity for the case where R is given by a Dirac delta function,

$$R(t) = A\,\delta(t - T), \tag{13}$$

and later generalise to an arbitrary response function. Expanding (11) in powers of Δ, keeping only the linear term, then using equation (13) for R and rearranging, one finds

$$v_\mathrm{d} = \lambda_0 \int_0^\infty dt\, \mathrm{e}^{-\lambda_0 t} E[w(t)] + \lambda_0^2 A |\nabla c| \int_0^\infty dt' \int_{t'}^\infty dt\, \mathrm{e}^{-\lambda_0 t} E[w(t) z(t' - T)], \tag{14}$$

where $w(t) = d\,z(t)/dt$. Writing $z(t)$ as an integral of $w(t)$, writing $w(t)$ as $v_\mathrm{s}\boldsymbol{e}(t).\hat{\boldsymbol{z}}$, (14) becomes

$$\begin{aligned} v_\mathrm{d} = {} & \lambda_0 \int_0^\infty dt\, \mathrm{e}^{-\lambda_0 t} \hat{\boldsymbol{z}} \cdot E[\boldsymbol{e}(t)] \\ & + \lambda_0^2 A |\nabla c| \int_0^\infty dt' \int_{t'}^\infty dt \int_0^{t'-T} dt''\, \mathrm{e}^{-\lambda_0 t} \hat{\boldsymbol{z}} \cdot E[\boldsymbol{e}(t)\boldsymbol{e}(t'')] \cdot \hat{\boldsymbol{z}}, \end{aligned} \tag{15}$$

Equation (15) contains the unknown terms $E[\boldsymbol{e}(t)]$ and $E[\boldsymbol{e}(t)\boldsymbol{e}(t'')]$. The calculation of these terms under different sets of assumptions is the subject of the following two sections.

5 Analytic calculation of v_d for a spherical organism

5.1 Derivation

For the case of a spherical organism, one can solve for v_d analytically, taking full account of temporal comparisons, persistence, and Brownian rotation. Once again, the method of solution is similar to that in Locsei [25], so just an outline of the derivation is sketched here.

First consider the case with no shear. In this case, the expected swimming direction for times $t > 0$ is

$$E[\boldsymbol{e}(t)] = \mathrm{e}^{-2D_\mathrm{R}t} E[\boldsymbol{e}(0^+)], \tag{16}$$

where $\boldsymbol{e}(0^+)$ is the cell's swimming direction at the beginning of the run [25]. The decaying exponential reflects the random re-orientation of the cell by Brownian rotation. The time autocorrelation function for swimming direction is

$$E[\boldsymbol{e}(t_2)\boldsymbol{e}(t_1)] = \begin{cases} \frac{1}{3}\mathrm{e}^{2D_\mathrm{R}(t_1-t_2)}\boldsymbol{1} & \text{if } 0 < t_1 < t_2 \\ \frac{\alpha_\mathrm{p}}{3}\mathrm{e}^{(2D_\mathrm{R}+\lambda_0[1-\alpha_\mathrm{p}])t_1}\mathrm{e}^{-2D_\mathrm{R}t_2}\boldsymbol{1} & \text{if } t_1 < 0 < t_2 \end{cases} \tag{17}$$

where $\boldsymbol{1}$ is the identity matrix. Note that the second case in (17) has a factor α_p due to the tumble at $t = 0$, an exponential decay term featuring D_R and λ_0 due to tumbles and Brownian rotation in the interval $t_1 < t < 0$, and an exponential decay term featuring just D_R due to Brownian rotation in the interval $0 < t < t_2$. For Reynolds numbers $\mathrm{Re} \ll 1$, a spherical object in a shear flow rotates with an angular velocity $\boldsymbol{\omega}$ equal to half the vorticity [23]. When shear is included, one can show that (16) and (17) generalise to

$$E[\boldsymbol{e}(t)] = \mathrm{e}^{-2\mathrm{D_R t}}\boldsymbol{R}(\mathrm{t}) \cdot \mathrm{E}[\boldsymbol{e}(0^+)], \tag{18}$$

and

$$E[\boldsymbol{e}(t_2)\boldsymbol{e}(t_1)] = \begin{cases} \frac{1}{3}\mathrm{e}^{2D_\mathrm{R}(t_1-t_2)}\boldsymbol{R}(t_2-t_1) & \text{if } 0 < t_1 < t_2 \\ \frac{\alpha_\mathrm{p}}{3}\mathrm{e}^{(2D_\mathrm{R}+\lambda_0[1-\alpha_\mathrm{p}])t_1}\mathrm{e}^{-2D_\mathrm{R}t_2}\boldsymbol{R}(t_2-t_1) & \text{if } t_1 < 0 < t_2 \end{cases} \tag{19}$$

where $\boldsymbol{R}(t)$ is the rotation matrix corresponding to a rotation by angle $|\boldsymbol{\omega}|t$ about the unit vector $\hat{\boldsymbol{\omega}}$.

It remains to find an expression for $E[\boldsymbol{e}(0^+)]$. Since the swimming direction after a tumble is chosen from an axisymmetric distribution around the swimming direction before the tumble, (4) gives

$$E[\boldsymbol{e}(0^+)] = \alpha_p E[\boldsymbol{e}(0^-)]. \tag{20}$$

Furthermore, if the cell has been swimming for a time $t_\mathrm{swim} \gg 1/\lambda_0$, then the expected swimming velocity just before a tumble does not change from one tumble to the next, so

$$\begin{aligned} E[\boldsymbol{e}(0^+)] &= \alpha_\mathrm{p} E[\boldsymbol{e}(t_\mathrm{f}^{\,-})] \\ &= \alpha_\mathrm{p}\int_0^t dt\, E[\boldsymbol{e}(t)p(t)]. \end{aligned} \tag{21}$$

After expanding $p(t)$ in powers of Δ and performing some simplification, one finds

$$E[\boldsymbol{e}(0^+)] = v_\mathrm{s}\lambda_0|\nabla c|A\left(\boldsymbol{B} - \frac{1}{\alpha_\mathrm{p}}\boldsymbol{1}\right)^{-1} \cdot (\boldsymbol{I}_1 - \boldsymbol{I}_2) \tag{22}$$

where

$$\boldsymbol{I}_1 = \int_0^\infty dt \int_0^{(t-T)} dt' \mathrm{e}^{-\lambda_0 t} E[\boldsymbol{e}(t)\boldsymbol{e}(t')], \tag{23}$$

$$\boldsymbol{I}_2 = \lambda_0 \int_0^\infty dt' \int_{t'}^\infty dt \int_0^{t'-T} dt'' \, \mathrm{e}^{-\lambda_0 t} E[\boldsymbol{e}(t)\boldsymbol{e}(t'')], \tag{24}$$

and

$$\boldsymbol{B} = \lambda_0 \int_0^\infty dt \mathrm{e}^{-(\lambda_0+2D_\mathrm{R})t}\boldsymbol{R}(t). \tag{25}$$

Now we have expressions for $E[\boldsymbol{e}(t)]$ and $E[\boldsymbol{e}(t)\boldsymbol{e}(t'')]$, and performing the necessary back-substitutions into (15) yields

$$v_\mathrm{d} = Ak_\mathrm{sphere}(T), \tag{26}$$

where

$$k_\mathrm{sphere}(T) = \frac{e^{-T(2D_\mathrm{R}+\lambda_0)}|\nabla c|v_\mathrm{s}^2(\alpha_\mathrm{p}-1)\lambda_0 b_1}{3[(2D_\mathrm{R}+\lambda_0)^2+\Omega^2][(2D_\mathrm{R}-\alpha_\mathrm{p}\lambda_0+\lambda_0)^2+\Omega^2]^2}, \tag{27}$$

with

$$b_1 = e^{T(2D_\mathrm{R}+\lambda_0)}\alpha_\mathrm{p}\lambda_0 b_2 - e^{T\alpha_\mathrm{p}\lambda_0}[(2D_\mathrm{R}+\lambda_0)^2+\Omega^2]b_3 \tag{28}$$

$$b_2 = (2D_\mathrm{R}+\lambda_0)(2D_\mathrm{R}-\alpha_\mathrm{p}\lambda_0+\lambda_0)^2 + [(2\alpha_\mathrm{p}-3)\lambda_0 - 6D_\mathrm{R}]\Omega^2 \tag{29}$$

$$\begin{aligned} b_3 = \; & [(2D_\mathrm{R}-\alpha_\mathrm{p}\lambda_0+\lambda_0)^2-\Omega^2]\cos\Omega T \\ & -2(2D_\mathrm{R}-\alpha_\mathrm{p}\lambda_0+\lambda_0)\Omega\sin\Omega T. \end{aligned} \tag{30}$$

The drift velocity for a general response function is then

$$v_\mathrm{d} = \int_0^\infty dT\, R(T)k_\mathrm{sphere}(T). \tag{31}$$

5.2 Consistency with known results

Equations (27) and (31) are consistent with existing literature in the appropriate limits. Locsei [25] considered chemotaxis in the absence of shear. When $\Omega = 0$, (27) simplifies to

$$k(T) = \frac{v_\mathrm{s}^2|\nabla c|\lambda_0\mathrm{e}^{-(\lambda_0+2D_\mathrm{R})T}(1-\alpha_\mathrm{p})[(\lambda_0+2D_\mathrm{R})\mathrm{e}^{\lambda_0\alpha_\mathrm{p}T} - \lambda_0\alpha_\mathrm{p}\mathrm{e}^{(\lambda_0+2D_\mathrm{R})T}]}{3(\lambda_0+2D_\mathrm{R})[\lambda_0(1-\alpha_\mathrm{p})+2D_\mathrm{R}]^2}, \tag{32}$$

consistent with [25]. Bearon and Pedley [5] calculated the chemotactic drift velocity for a spherical cell swimming in a uniform shear, under the assumption that the cell detects the chemoattractant gradient directly (rather than through temporal comparisons) and modifies its tumble rate according to

$$\lambda = \lambda_0(1-\varepsilon \boldsymbol{e}\cdot\hat{\boldsymbol{z}}), \tag{33}$$

with $|\varepsilon| \ll 1$. We note that within our framework (33) is equivalent to setting

$$R(t) = \frac{\varepsilon}{v_{\mathrm{s}}|\nabla c|}\frac{\delta(t-T)-\delta(t-T-\Delta t)}{\Delta t}, \tag{34}$$

and taking the simultaneous limits $\Delta t \to 0$ and $T \to 0$. Substituting (34) into (31) and taking the aforementioned limits, one finds the drift velocity for a gradient-detecting spherical organism:

$$v_{\mathrm{d}} = \frac{\varepsilon v_{\mathrm{s}}\lambda_0(\alpha_{\mathrm{p}}-1)[\lambda_0(\alpha_{\mathrm{p}}-1)-2D_{\mathrm{R}}]}{3[(\lambda_0(\alpha_{\mathrm{p}}-1)-2D_{\mathrm{R}})^2+\Omega^2]}. \tag{35}$$

Setting $\alpha_{\mathrm{p}} = 0$ and $D_{\mathrm{R}} = 0$, one finds

$$v_{\mathrm{d}} = \frac{\varepsilon v_{\mathrm{s}}\lambda_0^2}{3(\lambda_0^2+\Omega^2)}, \tag{36}$$

consistent with equation 30 of Bearon and Pedley [5].

5.3 Results: v_{d} for a spherical organism

Using response function (8), the drift velocity for a spherical organism in a shear flow is

$$\frac{v_{\mathrm{d}}}{\varepsilon v_{\mathrm{s}}} = \frac{(\alpha_{\mathrm{p}}-1)\lambda_0^3\{b_5[2D_{\mathrm{R}}-(\alpha_{\mathrm{p}}-2)\lambda_0]\Omega^2-b_4+b_6\}}{b_7} \tag{37}$$

where

$$b_4 = [4D_{\mathrm{R}}+(5-2\alpha_{\mathrm{p}})\lambda_0][2D_{\mathrm{R}}-(\alpha_{\mathrm{p}}-2)\lambda_0]^3(2D_{\mathrm{R}}-\alpha_{\mathrm{p}}\lambda_0+\lambda_0), \tag{38}$$

$$b_5 = 16D_{\mathrm{R}}^2+4(11-4\alpha_{\mathrm{p}})\lambda_0 D_{\mathrm{R}}+\left(4\alpha_{\mathrm{p}}^2-22\alpha_{\mathrm{p}}+25\right)\lambda_0^2, \tag{39}$$

$$b_6 = 3[4D_{\mathrm{R}}+(3-2\alpha_{\mathrm{p}})\lambda_0]\Omega^4, \tag{40}$$

and

$$b_7 = 9\{[(\alpha_{\mathrm{p}}-2)\lambda_0-2D_{\mathrm{R}}]^2+\Omega^2\}^3[(2D_{\mathrm{R}}-\alpha_{\mathrm{p}}\lambda_0+\lambda_0)^2+\Omega^2]. \tag{41}$$

Figure 2 shows the drift velocity v_{d} as a function of the shear strength Ω for a variety of persistence parameters α_{p}. As one might expect, the shear flow reduces the drift velocity. More surprisingly, the drift velocity is negative for sufficiently strong shear, so that the cell swims down the chemoattractant gradient rather than up it. Also, the larger the persistence parameter, the more susceptible the cell is to shear. For instance, with a persistence parameter of $\alpha_{\mathrm{p}} = -1$, v_{d} becomes negative for Ω beyond $\approx 1.5\ \mathrm{s}^{-1}$, whereas for $\alpha_{\mathrm{p}} = 0.78$, the drift velocity becomes negative for Ω beyond $\approx 0.4\ \mathrm{s}^{-1}$. Locsei [25] calculated that in the absence of

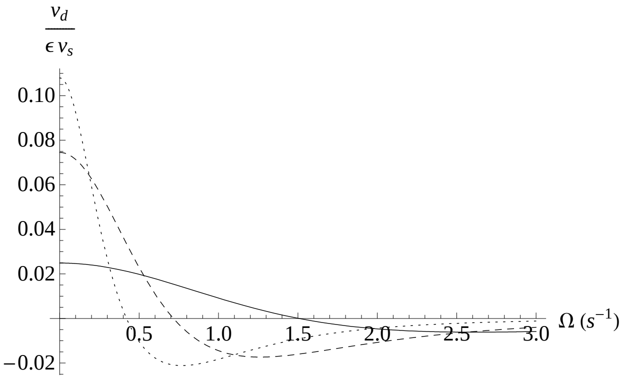

Fig. 2 Drift velocity versus shear strength, for persistence parameter $\alpha_{\rm p} = -1$ (solid line), $\alpha_{\rm p} = 0.33$ (dashed), and $\alpha_{\rm p} = 0.78$ (dotted), with $\lambda_0 = 1$ s^{-1} and $D_{\rm R} = 0.062$ radians^{2}s^{-1}. Note $\alpha_{\rm p} = 0.33$ is the measured value for *E. coli* [6].

shear, $\alpha_{\rm p} \approx 0.78$ is the value of persistence that maximises the drift velocity. In that paper, it was speculated that the measured persistence of $\alpha_{\rm p} \approx 0.33 < 0.78$ in real *E. coli* [6] might reflect a compromise between transient and steady state performance. The new results here suggest another reason why $\alpha_{\rm p} < 0.78$ for real *E. coli*: there is a compromise between performance in a stationary fluid and performance in a sheared fluid. Intuitively, the disadvantage of a high persistence parameter when performing chemotaxis in a sheared fluid arises because when a cell is rotated by the shear to face down the chemoattractant gradient, a single tumble is insufficient to reorient it to face up the gradient.

6 Semi-analytic calculation of $v_{\rm d}$ for an elongated organism

Whereas a spherical particle in a shear flow rotates with constant angular velocity, a non-spherical particle rotates with an angular velocity that depends on its instantaneous orientation. This complicates the calculation of drift velocity, but nonetheless one can still find an analytic integral expression for the drift velocity of a non-spherical cell in the absence of Brownian rotation and persistence, using the additional simplification of treating the cell as a prolate spheroid. In principle, one could include Brownian rotation and persistence in the calculation, but this would involve solving the full, time-dependent Fokker Plank equation, and we shall not attempt this here.

6.1 Modelling an *E. coli* cell as a prolate spheroid

In this section we show that an *E. coli* cell in a shear flow rotates in approximately the same manner as a prolate spheroid (ellipsoidal rod) of slenderness ratio $\eta \approx 9$, where η is defined as the ratio of major to minor axis.

We begin by considering the motion of a rigid body in a linear velocity field. A general, undisturbed linear velocity field $\boldsymbol{u}(\boldsymbol{x})$ has the form

$$\boldsymbol{u}(\boldsymbol{x}) = \boldsymbol{U} + \boldsymbol{\Omega} \times \boldsymbol{x} + \boldsymbol{E} \cdot \boldsymbol{x}, \tag{42}$$

where $\boldsymbol{U}$ is a uniform velocity, $\boldsymbol{\Omega}$ is an angular velocity equal to half the vorticity, and $\boldsymbol{E}$ is a second rank symmetric strain rate tensor. The shear flow considered in this paper is a special case of a linear flow, with

$$\begin{aligned} \boldsymbol{U} &= \boldsymbol{0}, \\ \boldsymbol{\Omega} &= (0, \Omega, 0), \\ \boldsymbol{E} &= \begin{pmatrix} 0 & 0 & \Omega \\ 0 & 0 & 0 \\ \Omega & 0 & 0 \end{pmatrix}, \end{aligned} \tag{43}$$

where $\Omega = \gamma/2$.

A swimming *E. coli* cell has a Reynolds number of $\mathrm{Re} \approx 10^{-5}$ [6] so the hydrodynamics of its motion are well described by Stokes flow. By the linearity properties of Stokes flow, the instantaneous angular velocity $\boldsymbol{\omega}$ of any rigid body in a linear flow takes the form

$$\omega_i = \Omega_i + B_{ijk} E_{jk} \tag{44}$$

(using the Einstein summation convention), where B_{ijk} is a dimensionless third rank constant tensor which is symmetric in its second and third indices, and the i, j, and k components refer to axes fixed in the body. For a sphere, $\boldsymbol{B} = \boldsymbol{0}$, reflecting the fact that a sphere does not rotate in a pure straining flow. Bretherton [11] showed that for a general axisymmetric body B_{ijk} has only a single free parameter. Taking the z axis to be aligned with the body's symmetry axis, an axisymmetric body has

$$\begin{aligned} -B_{123} = -B_{132} = B_{213} = B_{231} &= \alpha, \\ B_{ijk} = 0 \text{ for all other } &i, j, k. \end{aligned} \tag{45}$$

Bretherton [11] further showed that, provided $|\alpha| < 1$ (which is true for most physically realistic bodies), a body with B_{ijk} of the form (45) rotates in a shear flow in precisely the same way as a spheroid of slenderness ratio

$$\eta = \sqrt{(1+\alpha)/(1-\alpha)}. \tag{46}$$

This result is useful because the motion of a prolate spheroid in a shear flow was analysed by Jeffery [22], who showed that the motion consists of a closed orbit of simple analytical form, now commonly referred to as a 'Jeffery orbit'.

We shall consider a model *E. coli* cell composed of a spherical body rigidly attached to a helical flagellar bundle, modelled as a solid body of uniform circular cross-section, and show that despite the model cell being non-axisymmetric its B_{ijk} tensor is almost of the form (45). Our model cell consists of a sphere of radius a centered at the origin with respect to axes fixed in the cell and a left-handed helix of radius r, pitch (helical wavelength) h and length L, such that the position $\boldsymbol{x}$ at a point on the helix is given parametrically by

$$\boldsymbol{x}(\chi) = r(\boldsymbol{n}_1 \cos\chi - \boldsymbol{n}_2 \sin\chi) + \boldsymbol{n}_3 \left(a + \frac{h\chi}{2\pi}\right), \tag{47}$$

where $\chi \in [0, 2\pi L/h]$ and $\boldsymbol{n}_1, \boldsymbol{n}_2, \boldsymbol{n}_3$ are a right-handed set of unit vectors fixed in the cell such that $\boldsymbol{n}_3$ points along the helix axis away from the sphere.

It is sufficient to treat the helix and sphere as being fixed in position relative to one another, so that the cell is rigid rather than swimming. By the linearity property of Stokes flow, the angular velocity of a swimming cell in a shear flow is equal to the angular velocity of a swimming cell in a stationary fluid, plus the angular velocity of a rigid cell in a shear flow. Since $\Omega_1 = \Omega_2 \approx 0$ for a swimming cell in a stationary fluid (because the cell swims in an approximately straight line), Ω_1 and Ω_2 are the same for a swimming cell in a shear flow as for a rigid cell in a shear flow. Ω_3 is not relevant to calculations of drift velocity, since rotation about $\boldsymbol{n}_3$ does not alter the swimming direction.

For a given background flow, the translational velocity $\boldsymbol{V}$ and angular velocity $\boldsymbol{\omega}$ of the body are found by setting the net force and net torque on the body to zero. We neglect the interaction of flows around the helix and the sphere. For a given motion of the cell through a given background velocity field, we assume that the total viscous force on the cell is simply the force on the sphere in the absence of the helix plus the force on the helix in the absence of the sphere, and we similarly assume simple addition of the viscous torques. This is not an unreasonable approximation since the body diameter (1–2μm) is a small fraction of flagellar bundle length (5–10μm). To calculate the force and torque on the sphere, we use the well known exact expressions [see for instance 2]. To calculate the force and torque on the helix we use resistive force theory [18], which assumes that the components of the viscous force on an element of the helix are proportional to the same components of the fluid's velocity relative to that element, but with different coefficients of proportionality for normal and tangential components. Various pairs of coefficients have been proposed for a simple flagellum of uniform circular cross-section, and we use the more accurate coefficients due to Lighthill [24] rather than the original coefficients proposed by Gray and Hancock [18]. These coefficients have as parameters the helix pitch h and the cross-sectional radius b of the helix bundle. Resistive force theory is a crude approximation of true flagellar hydrodynamics, since it ignores interactions between neighbouring elements of the flagellum, but it has nonetheless been shown to give reasonable results when applied to swimming spermatozoa, for example [24].

Given the above method for calculating the motion of the body in a given flow, one can determine the B_{ijk} tensor from (44) by setting $\boldsymbol{\Omega} = \boldsymbol{0}$ and considering the angular velocity $\boldsymbol{\omega}$ that results from each of the following elementary strain matrices, in which all E_{ij} except those mentioned are zero: $E_{11} = 1$; $E_{22} = 1$; $E_{33} = 1$; $E_{12} = E_{21} = 1$; $E_{23} = E_{32} = 1$; $E_{31} = E_{13} = 1$.

In principle one can determine B_{ijk} in symbolic form with a, b, r, L, and h as parameters, but in practice the algebra required to perform this task is unwieldy and so one must choose numerical values for the parameters before calculating B_{ijk}. A typical *E. coli* cell body is rod shaped with a diameter of $\approx 1\mu$m and a length of $\approx 2\mu$m, and possesses about 6 flagella [6]. The length of each flagellum is typically in the range 5–10μm, and the diameter of each flagellar filament is $\approx$ 20nm [28, pp. 70–83]. The pitch of the helix is $\approx 2.5\mu$m and the helix radius is $\approx 0.25\mu$m [32]. On the basis of these measurements, we take the dimensions of our model cell to be $a = 0.7\mu$m, $r = 0.25\mu$m, $L = 8\mu$m, $h = 2.5\mu$m, $b = \sqrt{6} \times$ 10nm. With these dimensions, calculation of the B_{ijk} reveals that, for the model cell, they come close to possessing the properties expected for an axisymmetric body [eq. (45)], in that

$$\begin{aligned} -B_{123} = -B_{132} \approx B_{213} = B_{231} &\approx 0.974, \\ B_{333} &\approx 0.501, \\ |B_{ijk}| < 0.05 \text{ for all other } i, j, k&. \end{aligned} \tag{48}$$

The most notable breaking of symmetry is that B_{333} is not small (whereas it is zero for an axisymmetric body) but this only affects Ω_3 and thus has no bearing on the swimming direction. All other elements of B_{ijk} that are zero for an axisymmetric body have magnitude < 0.05 for the model cell (and all but one, $B_{133} = -0.0445$, have magnitude ≤ 0.01), so discrepancies between the angular velocities of the model cell and an 'equivalent spheroid' are of order 5%. Using (46), the slenderness ratio of the 'equivalent spheroid' that rotates in a similar manner to the model cell is $\eta \approx 9$. For other plausible values of a and L, η ranges from $\eta \approx 4$ (for $a = 1\mu$m, $L = 5\mu$m) to $\eta \approx 15$ (for $a = 0.5\mu$m, $L = 10\mu$m).

6.2 Integral expression for drift velocity of prolate spheroid

Neglecting Brownian rotation and persistence, one can find an analytic integral expression for the drift velocity. The direction faced at the beginning of each run is taken from the uniform distribution on the unit sphere, so by symmetry $E[\boldsymbol{e}(t)] = \boldsymbol{0}$ and the first term in (15) vanishes. Also, since any correlation in swimming direction is destroyed by the tumble, $E[\boldsymbol{e}(t)\boldsymbol{e}(t'')] = \boldsymbol{0}$ for $t'' < 0 < t$, which allows some simplification of the second term in (15). One finds

$$v_{\mathrm{d}} = \frac{\lambda_0^2 A|\nabla c|}{v_{\mathrm{s}}^2} \int_T^\infty dt\, \mathrm{e}^{-\lambda_0 t} \int_0^{(t-T)} dt' \, (t - t' - T) E[w(t)w(t')]. \tag{49}$$

It remains to find an expression for the velocity autocorrelation function $E[w(t)w(t')]$.

Since it was established in section 6.1 that an *E. coli* cell rotates in a shear flow with very nearly the same angular velocity as a prolate spheroid, we henceforth treat the cell as a prolate spheroid that swims along its long axis. Define direction angles θ and ϕ such that

$$\boldsymbol{e} \cdot \hat{\boldsymbol{z}} = \sin\theta \cos\phi \tag{50}$$

$$\boldsymbol{e} \cdot \hat{\boldsymbol{x}} = \sin\theta \sin\phi \tag{51}$$

$$\boldsymbol{e} \cdot \hat{\boldsymbol{y}} = \cos\theta. \tag{52}$$

In a shear flow, neglecting Brownian rotation, the cell follows Jeffery orbits, and the angles θ and ϕ evolve according to [22]

$$\tan\phi = \eta \tan(\sigma t - \beta_0), \tag{53}$$

$$\tan^2\theta = \frac{\eta^2}{\kappa_0(\eta^2 \cos^2\phi + \sin^2\phi)}, \tag{54}$$

where κ_0 and β_0 are constants of integration depending on the initial orientation, and

$$\sigma = \frac{2\Omega\,\eta}{\eta^2+1}. \tag{55}$$

In terms of the initial orientation angles θ_0 and ϕ_0 at time $t = 0$, the constants of integration are

$$\begin{aligned} \beta_0(\phi_0) &= -\arctan(\eta\cos\phi_0, \sin\phi_0), && (56)\\ \kappa_0(\theta_0,\phi_0) &= \frac{\eta^2}{\tan^2\theta_0(\eta^2\cos^2\phi_0+\sin^2\phi_0)}, && (57) \end{aligned}$$

where the arctan function is treated as taking two arguments so as to return an answer in the correct quadrant. For instance, if $\psi = \arctan(x_1,x_2)$, then $\cos\psi = x_1(x_1^2+x_1^2)^{-1/2}$ and $\sin\psi = x_2(x_1^2+x_1^2)^{-1/2}$.

Let $w(t;\boldsymbol{e}_0)$ be the cell's velocity projected along the z axis at a time $t \geq 0$, given that the cell's swimming direction at the beginning of the run was $\boldsymbol{e}_0$. Manipulation of (50), (53) and (54) gives

$$\begin{aligned} w(t;\boldsymbol{e}_0) &= v_{\mathrm{s}}\sin\theta\cos\phi \\ &= \frac{v_{\mathrm{s}}\cos(\sigma t-\beta_0)}{\left[\kappa_0+\cos^2(\sigma t-\beta_0)+\eta^2\sin^2(\sigma t-\beta_0)\right]^{1/2}}. \end{aligned} \tag{58}$$

$E[w(t_1)w(t_2)]$ may be written as an explicit average over all possible initial run directions:

$$E[w(t_1)w(t_2)] = \frac{1}{4\pi}\int_0^\pi d\theta_0\sin\theta_0\int_0^{2\pi} d\phi_0\, w(t_1;\boldsymbol{e}_0)w(t_2;\boldsymbol{e}_0), \tag{59}$$

where the integrand is treated as a function of θ_0 and ϕ_0. Using (56), we can transform this last equation into to

$$E[w(t_1)w(t_2)] = \frac{\eta}{4\pi}\int_0^\pi d\theta_0\sin\theta_0\int_0^{2\pi} d\beta_0\frac{w(t_1;\boldsymbol{e}_0)w(t_2;\boldsymbol{e}_0)}{\cos^2\beta_0+\eta^2\sin^2\beta_0}, \tag{60}$$

where the integrand is now treated as a function of θ_0 and β_0, and there is an accompanying expression for κ_0 in terms of θ_0 and β_0 instead of θ_0 and ϕ_0:

$$\kappa_0(\theta_0,\beta_0) = \frac{\cos^2\beta_0+\eta^2\sin^2\beta_0}{\tan^2\theta_0}. \tag{61}$$

Equations (58), (60), and (61) now give a complete expression for $E[w(t_1)w(t_2)]$. The right hand side of (60) cannot be integrated analytically for general η, but can be evaluated by numerical quadrature. In the limit of weak shear, one can expand the integrand in powers of Ω/λ_0, taking t_1 and t_2 to be of order $1/\lambda_0$, and integrate to find

$$\begin{aligned} E[w(t_1)w(t_2)] = \frac{v_{\mathrm{s}}^2}{3} - \frac{2v_{\mathrm{s}}^2\Omega^2}{105(\eta^2+1)^2}\{&-2(3\eta^4+8\eta^2+24)t_1t_2 \\ &+(12\eta^4+11\eta^2+12)(t_1^2+t_2^2)\} + O(\Omega^4/\lambda_0^4). \end{aligned} \tag{62}$$

Note that (62) contains only even powers of Ω since by symmetry the drift velocity does not depend on the sign of Ω.

For a general response function, the drift velocity is given by

$$v_\mathrm{d} = \int_0^\infty dT\, R(T) k_\mathrm{spheroid}(T), \tag{63}$$

where

$$k_\mathrm{spheroid}(T) = \frac{\lambda_0^2 |\nabla c|}{v_\mathrm{s}^2} \int_T^\infty dt\, \mathrm{e}^{-\lambda_0 t} \int_0^{(t-T)} dt'\, (t - t' - T) E[w(t)w(t')], \tag{64}$$

with $E[w(t)w(t')]$ given by (60).

6.3 Consistency with known results

de Gennes [14] calculated the chemotactic drift velocity in the absence of a shear flow, and without Brownian rotation or persistence. Setting $\Omega = 0$, the velocity autocorrelation function is simply $E[w(t_1), w(t_2)] = v_\mathrm{s}^2/3$, and (64) and (63) reduce to

$$v_\mathrm{d} = \frac{v_\mathrm{s}^2 |\nabla c|}{3\lambda_0} \int_0^\infty R(t) \mathrm{e}^{-\lambda_0 t} dt, \tag{65}$$

consistent with equation 16 of de Gennes [14]. As mentioned in section 5.2, Bearon and Pedley [5] calculated the chemotactic drift velocity for a spherical cell swimming in a uniform shear, under the assumption that the cell detects the chemoattractant gradient and modifies its tumble rate according to (33). We can treat this case as follows. For a sphere, $\eta = 1$, and the velocity autocorrelation function simplifies to

$$E[w(t_1), w(t_2)] = \frac{v_\mathrm{s}^2}{3} \cos[\Omega(t_1 - t_2)], \tag{66}$$

and substitution of (66) into (64) yields

$$k(T) = -\frac{\mathrm{e}^{-\lambda_0 T} [(\Omega^2 - \lambda_0^2)\cos \Omega T + 2\Omega \sin \Omega T]}{3(\lambda_0^2 + \Omega^2)^2}. \tag{67}$$

As in section 5.2, gradient detection is modelled by using the response function (34) and taking the appropriate limits, and one finds that once again the drift velocity reduces to (36), consistent with [5].

6.4 Results: v_d for an elongated organism

For weak shear ($\Omega \ll \lambda_0$), we can substitute (62) and (8) into (64) and (63) to find

$$\frac{v_\mathrm{d}}{\varepsilon v_\mathrm{s}} = \varepsilon \left[\frac{5}{72} - \frac{\Omega^2}{\lambda_0^2} g(\eta) + O\left(\frac{\Omega^4}{\lambda_0^4}\right) \right] \tag{68}$$

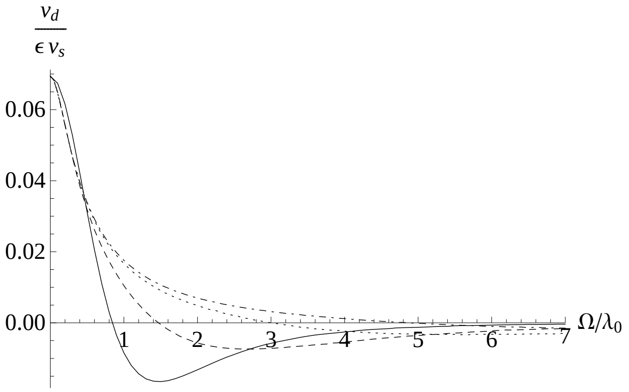

Fig. 3 Drift velocity v_d as a function of the shear strength parameter Ω for equivalent slenderness ratios $\eta = 1$ (solid line), $\eta = 4$ (dashed line), $\eta = 9$ (dotted line), and $\eta = 15$ (dot-dashed line).

where

$$g(\eta) = \frac{243\eta^4 + 151\eta^2 - 44}{420(1+\eta^2)^2}. \tag{69}$$

Note that $g(\eta)$ is bounded and monotonically increasing for $\eta > 0$, with $g(\infty) = 81/140$. In fact, $g(4) \approx 0.92 g(\infty)$, indicating that for $\Omega \ll 1$ and $\eta > 4$, v_d is approximately independent of η.

For general Ω and η, no analytic simplifications are possible and we evaluate the integral (63) numerically using the 'Cuba' integration library developed by Hahn [20]. Figure 3 shows the drift velocity v_d as a function of the shear strength Ω for a range of values of the slenderness ratio η. Note that for $\Omega < 0.5$ and $\eta \geq 4$, v_d is approximately independent of η, consistent with the analysis in the previous paragraph. Also, for any given η, and for sufficiently large Ω, the cell exhibits 'negative chemotaxis' *i.e.* v_d is negative. For instance, if $\eta = 9$ then $v_\mathrm{d} < 0$ for $\Omega > 3$. The minimum value of Ω for which $v_\mathrm{d} < 0$ depends on η; for larger η, v_d remains positive up to a larger value of Ω.

This last finding can be explained as follows. A key feature of the Jeffery orbit of a prolate spheroid with large slenderness ratio is that that there are lengthy 'pauses' with the spheroid's symmetry axis almost parallel to the streamlines, but the orientation reverses periodically. From (53) and (55) we see that the period $T_\mathrm{Jef.}$ of a Jeffery orbit is

$$T_\mathrm{Jef.} = \pi(\eta^2+1)/(\Omega\eta), \tag{70}$$

which is a monotonically increasing function of η for $\eta > 1$. Let Ω_crit be the lowest value of Ω for which $v_\mathrm{d} = 0$. In order for v_d to be less than or equal to zero, the sign of w must change during a typical run, and thus $T_\mathrm{Jef.}$ must be comparable to or smaller than the mean run duration $1/\lambda_0$. Thus, we expect that the dependence of Ω_crit on η scales roughly as

$$\Omega_\mathrm{crit}/\lambda_0 \sim q(\eta) \equiv (\eta^2+1)/\eta. \tag{71}$$

In fact, we find that $(\Omega_\mathrm{crit}/\lambda_0)/q(\eta) = 0.42, 0.35, 0.33, 0.32$ for $\eta = 1, 4, 8, 16$ respectively, indicating that the scaling (71) is approximately correct.

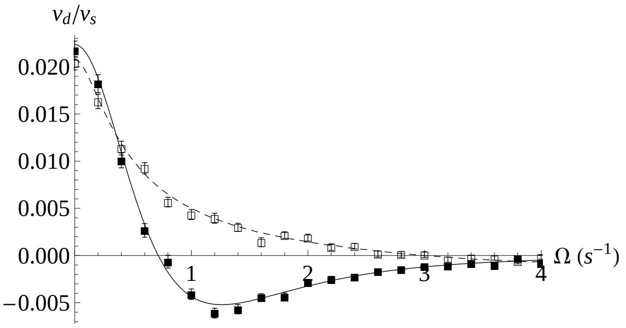

Fig. 4 Examples of agreement between analytic theory and Monte Carlo simulation results. Solid line shows analytic result for a spherical organism with $\alpha_{\rm p} = 0.33$, $D_{\rm R} = 0.062$ radians^{2}s^{-1}, $\varepsilon = 0.3$, and $\lambda_0 = 1$ s^{-1}; solid squares are Monte Carlo results for the same set of parameters. Dashed line shows analytic result for an elongated organism with $\eta = 9$, $\alpha_{\rm p} = 0$, $D_{\rm R} = 0$ radians^{2}s^{-1}, $\varepsilon = 0.3$, and $\lambda_0 = 1$ s^{-1}; empty squares show Monte Carlo results for the same set of parameters. Error bars show the standard error of the mean for Monte Carlo results.

7 Calculation of $v_{\rm d}$ by Monte Carlo simulation

The purpose of using Monte Carlo simulation here is twofold. First, it gives a means of checking the analytic results derived in earlier sections. Second, it allows us to calculate $v_{\rm d}$ in the regime which was not analytically tractable, namely the regime including all four effects of (i) temporal comparisons, (ii) persistence, (iii) Brownian rotation, and (iv) elongated cell shape. One can then check that the conclusions drawn from the analytic calculations are still valid when all four effects are taken into account.

7.1 Monte Carlo algorithm and test cases

The algorithm for calculating $v_{\rm d}$ by Monte Carlo simulation is straightforward. For each set of parameter values, 100 simulations are run, each of duration $10^4/\lambda_0$. Time is discretised into steps of size $\Delta t = 0.01/\lambda_0$. At each time step, the tumble probability (1) is evaluated by numerical quadrature, and a random number generator is used to decide whether the cell tumbles. If the cell tumbles, then the new direction is chosen from an axisymmetric distribution about the old direction, such that the new direction makes an angle of $\arccos(\alpha_{\rm p})$ with the old direction. If the cell doesn't tumble, then Brownian rotation is simulated by giving the cell a new direction chosen from an axisymmetric distribution about the old direction, such that the new direction makes an angle of $\arccos(1 - 2D_{\rm R}\Delta t) \approx 2\sqrt{D_{\rm R}\Delta t}$ with the old direction, and in addition the cell's position and direction of motion is incremented according to the Jeffery orbit equations [22]. A computer code was written to implement the above algorithm, and its output was compared to the analytic results derived in earlier sections. As show in figure 4, the analytic and simulation results agree well.

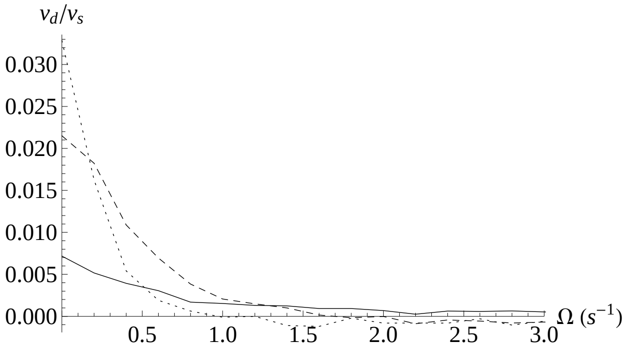

Fig. 5 Monte Carlo results for drift velocity v_{d} as a function of shear strength Ω, for persistence parameters of $\alpha_{\mathrm{p}} = -1$ (solid line), $\alpha_{\mathrm{p}} = 0.33$ (dashed), and $\alpha_{\mathrm{p}} = 0.78$ (dotted). In each case, $\eta = 9$, $D_{\mathrm{R}} = 0.062$ radians^{2}s^{-1}, $\lambda_0 = 1$ s^{-1} and $\varepsilon = 0.3$. Standard errors (not shown) are of the same magnitude as those in figure 4.

7.2 The effect of persistence on drift velocity

In section 5.3, it was shown that for a spherical organism, a higher persistence α_{p} results in a greater drift velocity v_{d} in the absence of shear, but a lower drift velocity in higher values of shear (figure 2). Using the Monte Carlo code, the same calculation was repeated, but for an elongated organism ($\eta = 9$). As shown in figure 5, the results remain qualitatively similar. For instance, $\alpha_{\mathrm{p}} = 0.78$ gives a higher v_{d} than $\alpha_{\mathrm{p}} = 0.33$ for shear rates up to $\Omega \approx 0.2$ s^{-1}, but for shear rates beyond that the situation is reversed. The main difference between figures 2 and 5 is that when elongated cell shape is taken into account, v_{d} never becomes as strongly negative as it does in the case of a spherical organism.

7.3 The effect of organism shape on drift velocity

In section 6.4, it was shown that a more elongated organism (larger η) is able to perform chemotaxis in stronger shear flows than a less elongated organism (figure 3), in the case where persistence and Brownian rotation are neglected. Using the Monte Carlo code, the same calculation was repeated, but including persistence ($\alpha_{\mathrm{p}} = 0.33$) and Brownian rotation ($D_{\mathrm{R}} = 0.062$ radians^{2}s^{-1}). As shown in figure 6, the results remain qualitatively unchanged. For instance, for $\eta = 1$, v_{d} remains positive for shear rates up to $\Omega \approx 0.8$ s^{-1}, whereas for $\eta = 9$, v_{d} remains positive for shear rates up to $\Omega \approx 1.5$s^{-1}. However, the effect of η is less pronounced than in the case where persistence and Brownian rotation are neglected. The physical reason for this is as follows. In the absence of Brownian rotation, an elongated cell ($\eta \gg 1$) has a lengthy ‘pause’ when it is almost parallel to the streamlines of the shear flow. The larger the value of η, the longer the pause, and the more robust v_{d} is in the face of shear. However Brownian rotation ‘jostles’ the cell out of alignment with the streamlines, puts a limit on the duration of the pause, and consequently reduces the robustness of v_{d} in the face of shear.

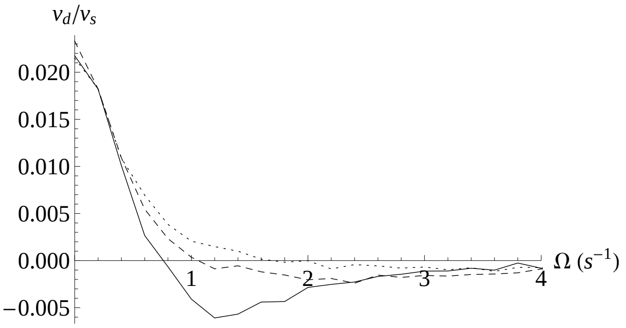

Fig. 6 Monte Carlo results for drift velocity v_d as a function of shear strength Ω, for slenderness ratios of $\eta = 1$ (solid line), $\eta = 4$ (dashed), and $\eta = 9$ (dotted). In each case, $\alpha_\mathrm{p} = 0.33$, $D_\mathrm{R} = 0.062$ radians^{2}s^{-1}, $\lambda_0 = 1$ s^{-1} and $\varepsilon = 0.3$. Standard errors (not shown) are of the same magnitude as those in figure 4. Results for $\eta = 15$ are statistically indistinguishable from results for $\eta = 9$ (data not shown).

8 Discussion and Conclusion

In this paper we have used a combined analytic and numeric approach to calculate the drift velocity v_d of a cell performing run and tumble chemotaxis in a uniform shear flow, taking account of (i) temporal comparisons performed by the cell, (ii) persistence of direction, (iii) Brownian rotation, and (iv) cell geometry. Our key findings are that (a) shear reduces the drift velocity, and a sufficiently strong shear may cause the cell to perform negative chemotaxis and swim down the chemoattractant gradient rather than up it, (b) in terms of maximising drift velocity, a high persistence parameter is advantageous in a quiescent fluid but disadvantageous in a shear flow, and (c) a more elongated body shape is advantageous in performing chemotaxis in a strong shear flow.

Temporal comparisons of chemoattractant concentration performed by the cell constitute a form of time delay in its response. The cell biases its tumble rate according to the history of chemoattractant concentration it has experienced, rather than according to the instantaneous concentration or concentration gradient. Negative chemotaxis arises from the combination of this time delay with rotation by the shear flow. For instance, a cell may commence swimming up the chemoattractant gradient on a particular run, but be rotated by the shear flow to swim down the gradient. Due to the time-delay in its response, the cell responds as if it were still swimming up the gradient, so it extends the length of the run, even though the net displacement is down the gradient. Conversely, a run with a net displacement up the chemoattractant gradient may be foreshortened. Lengthened runs down the gradient and foreshortened runs up the gradient lead to negative chemotaxis. Note that negative chemotaxis does not occur for an organism that responds to the instantaneous chemoattractant gradient; the drift velocity given by (35) is non-negative.

The possibility of negative chemotaxis was already derived by Bearon and Pedley [5], although the authors did not comment on it explicitly. They calculated the drift velocity for a spherical cell performing run and tumble chemotaxis in a shear flow, and investigated a form of time delay in the cell's response. In their model, a cell could bias its tumble rate according to either the present angle between the swimming direction and the chemoattractant gradient (no delay), or the original angle between the swimming direction and the chemoattractant gradient at the beginning of the run (delay). The authors found that in the delay case the drift velocity was significantly more reduced by shear than in the no-delay case, and equation 27 of their paper shows that in the delay case the drift velocity becomes negative for sufficiently large shear.

The present study shows that in terms of maximising drift velocity, a high persistence parameter is advantageous in a quiescent fluid but disadvantageous in a sufficiently strong shear flow. Locsei [25] previously showed that there is a synergy between temporal comparisons and persistence, and that when temporal comparisons are taken into account the drift velocity in a quiescent fluid is maximised by a persistence parameter $\alpha_\mathrm{p} \approx 0.78$, which is greater than the observed value of $\alpha_\mathrm{p} \approx 0.33$. In that paper, it was suggested that the discrepancy between the observed and apparently optimal values of α_p was due to a compromise between transient and steady-state behaviour, with lower values of α_p favouring steady state behaviour. The results of the present study suggest that the observed persistence $\alpha_\mathrm{p} \approx 0.33$ may reflect an additional trade-off between performance in a quiescent fluid and performance in a sheared fluid.

The present study also shows that the elongated shape of an *E. coli* cell works to its advantage in terms of performing chemotaxis in a shear flow, particularly if the rotational diffusivity is zero or small. A more elongated body has a longer Jeffery orbit period in a shear flow, and this reduces the likelihood that the shear flow rotates it from facing up the gradient to down the gradient or vice-versa in any given run. Thus, a more elongated body maintains a positive drift velocity up a larger value of shear strength Ω than a less elongated body. This effect is still present, but less pronounced, when rotational diffusivity is accounted for, because the rotational diffusivity perturbs the Jeffery orbits.

It is worth mentioning that the influence of bacterial shape and persistence of direction on chemotaxis in a moving fluid has been investigated in a slightly different context by Luchsinger et al [26]. In their oceanographically-motivated paper they numerically modelled bacteria clustering around a localised nutrient source in a straining flow. They showed that the tendency of an elongated bacterial cell to align with the direction of the straining flow assists it to remain near the nutrient source. Furthermore, they showed that a ‘back and forth’ motion ($\alpha_\mathrm{p} = -1$) is superior to a run and tumble motion ($\alpha_\mathrm{p} = 0$) in this context, because it allows the cell to maintain its alignment with the straining flow. Their work in conjunction with the present study illustrates that the ‘optimal’ values for chemotaxis parameters depend on context; a strategy that works well for locating a localised nutrient source may be different from a strategy that works well for swimming up a uniform nutrient gradient.

In conclusion, we should note that while the present work aimed to improve the realism of previous studies by including effects that were previously omitted, the model is still somewhat idealised and this should be born in mind when interpreting the results. More work, both theoretical and experimental, needs to be done to understand bacterial chemotaxis in realistic flow conditions. For example, one of the original motivations of this research was to derive the drift velocity and effective self-diffusivity for populations of bacteria in a general linear flow

(42), not just a simple shear directed perpendicular to the local chemoattractant gradient [3]. This remains a future goal. In addition, experiments indicate that in certain conditions boundary effects play an important role and even allow bacteria to swim upstream [21], and the fluid dynamics of this are not fully understood. Finally, we note that one of the strongest motivations for studying bacterial chemotaxis in moving fluids is to understand the role of marine bacteria in the pelagic food web, and yet while it is known that marine bacteria are able to swim faster and react more rapidly to chemical stimuli than *E. coli* [27, 1], their chemotactic response has yet to be thoroughly characterised and this must be done before modelling can proceed on a firm footing.

The authors are grateful for enlightening discussions with John Rallison, Ray Goldstein, Howard Berg, Henry Fu, Roman Stocker, Marcos, and Rachel Bearon.

References

1. Barbara GM, Mitchell JG (2003) Bacterial tracking of motile algae. FEMS Microbiol Ecol 44(1):79–87
2. Batchelor GK (1967) An Introduction to Fluid Dynamics. Cambridge University Press
3. Bearon RN (2001) Run-and-tumble chemotaxis in an ambient fluid flow. PhD thesis, University of Cambridge
4. Bearon RN (2003) An extension of generalized Taylor dispersion in unbounded homogeneous shear flows to run-and-tumble chemotactic bacteria. Physics of Fluids 15(6):1552–1563
5. Bearon RN, Pedley TJ (2000) Modelling run-and-tumble chemotaxis in a shear flow. Bull Math Biol 62:775–791
6. Berg HC (1983) Random Walks in Biology. Princeton University Press
7. Berg HC (2007) personal communication
8. Berg HC, Brown DA (1972) Chemotaxis in *Escherichia coli* analysed by three-dimensional tracking. Nature 239:500–504
9. Block SM, Segall JE, Berg HC (1982) Impulse responses in bacterial chemotaxis. Cell 31:215–226
10. Bowen JD, Stolzenbach KD, Chisholm SW (1993) Simulating bacterial clustering around phytoplankton cells in a turbulent ocean. Limnol Oceanogr 38(1):36–51
11. Bretherton FP (1962) The motion of rigid particles in a shear flow at low Reynolds number. J Fluid Mech 14:284–304
12. Clark DA, Grant LC (2005) The bacterial chemotactic response reflects a compromise between transient and steady-state behavior. Proc Nat Acad Sci USA 102(26):9150–9155
13. Costerton JW, Lewandowski Z (1995) Microbial biofilms. Annu Rev Microbiol 49:711–745
14. de Gennes PG (2004) Chemotaxis: the role of internal delays. Eur Biophys J 33:691–693
15. Erban R, Othmer HG (2004) From individual to collective behaviour in bacterial chemotaxis. SIAM J Appl Math 65(2):361–391

16. Erban R, Othmer HG (2005) From signal transduction to spatial pattern formation in *E. coli*: a paradigm for multiscale modeling in biology. Multiscale Model Simul 3(2):362–394
17. Fu H (2007) personal communication
18. Gray J, Hancock GJ (1955) The propulsion of sea-urchin spermatozoa. J Exp Biol 32:802–814
19. Grossart HP, Riemann L, Azam F (2001) Bacterial motility in the sea and its ecological implications. Aquat Microb Ecol 25:247–258
20. Hahn T (2005) Cuba—a library for multidimensional numerical integration. Comput Phys Commun 168:78–95
21. Hill J, Kalkanci O, McMurry JL, Koser H (2007) Hydrodynamic surface interactions enable escherichia coli to seek efficient routes to swim upstream. Phys Rev Lett 98(6):068,101–+
22. Jeffery GB (1922) The motion of ellipsoidal particles immersed in a viscous fluid. Proc R Soc Lond A 102:161–179
23. Kim S, Karrila SJ (1992) Microhydrodynamics: Principles and Selected Applications. Butterworth Heinemann
24. Lighthill J (1976) Flagellar hydrodynamics. SIAM Rev 18(2):161–230
25. Locsei JT (2007) Persistence of direction increases the drift velocity of run and tumble chemotaxis. J Mol Biol 55(1):41–60
26. Luchsinger RH, Bergerson B, Mitchell JG (1999) Bacterial swimming strategies and turbulence. Biophys J 77:2377–2386
27. Mitchell JG, Pearson L, Dillon S (1996) Clustering of marine bacteria in seawater enrichments. Appl Environ Microbiol 62(10):3716–3521
28. Neidhardt FC (ed) (1987) *Escherichia coli* and *Salmonella typhimurium*: Cellular and Molecular Biology, vol 1. Am. Soc. Microbiol., Washington, DC
29. Schnitzer MJ (1993) Theory of continuum random walks and applications to chemotaxis. Phys Rev E 48(4):2553–2568
30. Segall JE, Manson MD, Berg HC (1982) Signal processing times in bacterial chemotaxis. Nature 296:855–857
31. Segall JE, Block SM, Berg HC (1986) Temporal comparisons in bacterial chemotaxis. Proc Nat Acad Sci USA 83(23):8987–8991
32. Turner L, Ryu WS, Berg HC (2000) Real-time imaging of fluorescent flagellar filaments. J Bacteriol 182(10):2793–2801
33. Young KD (2006) The selective value of bacterial shape. Microbiol Mol Biol Rev 70(3):660–703, DOI 10.1128/MMBR.00001-06